2026 IEEE/SICE International Symposium on System Integration (SII)
January 11-14, 2026. Cancún, México

# Design Analysis of Tendon-Actuated Soft Robot for Colonoscopy

Ibrahim A. Seleem[1*,2] and Hiroshi Takemura[1]

*Abstract*— **Endoscopic-based double balloon represents an advanced technique for diagnosing and treating bowel cancer. However, existing designs face challenges including complexity and high cost due to the use of hybrid actuation, leading to prolonged procedure duration and patients' pain. This article introduces a novel design of a multi-section soft robot actuated by cables. It is composed of two sections, each capable of bending in two planes. Additionally, the distal section can perform compression and extension. Four tendons separated by 90° are used to control the bending of each section. Each pair of parallel cables is attached to a DC motor through a double-groove pulley. Moreover, four independent cables are utilized to compress and extend the distal section. Finite element analysis is conducted to evaluate the performance of the prototype concerning its bending and displacement. Experimental validation is carried out to investigate the capability of the design in terms of bending and payload capacity. The results show that the robot can bend by more than 270° under a payload of 50 g. This paper represents the first phase for developing a soft colonoscope and relaxing the complexity of current designs.**

## I. INTRODUCTION

In Japan, colorectal cancer (CRC) is among the most common types of cancer, with a significant rise in patients and deaths over time, driven by lifestyle factors and an aging population [1], [2]. Its late detection led to side effects and increased pain. In contrast, early diagnosis reduces side symptoms and healthcare costs, with more than 60% of an average 5-year survival rate [3]. Traditional colonoscopy is a well-known technique for examining the bowel and removing lesions. It uses a flexible long rod and a control mechanism at the tip, which contains a camera, lights, and tools for removing tumors. However, navigation through the lower gastrointestinal tract often requires forcible insertion, which causes pain and discomfort for the patient and may lead to perforation of the colonic mucosa [4]. To address these challenges, double balloon endoscopy was developed to perform deep insertion and improve the access to the small intestine [5]. Figure 1 illustrates that it consists of a colonoscope and overtube with two inflatable balloons, which are sequentially inflated and deflated to the intestinal wall.

Inspired by the locomotion of biological appendages such as inchworms, researchers have developed soft colonoscope to enhance safety and allow dexterous movement. A pneumatically actuated inchworm-like soft robot for endoscopy was developed in [7]. It was composed of a set of bracing balloons, fixed at the proximal and distal ends of a rigid polymer tube, which expanded radially to generate attraction forces. Additionally, a middle actuation balloon was utilized to allow bending and maneuvering. An internal helical NiTi coil was used to avoid buckling during motion. In [8], a design of three sections earthworm inspired soft robot for gastrointestinal inspection was introduced. Two balloons fabricated from silicone resin were attached to the head and rear sections. By controlling three pneumatic tubes distributed around the middle section, the prototype was able to bend, expand, and compress. However, these designs suffer from limited bending angles and low payload capacity.

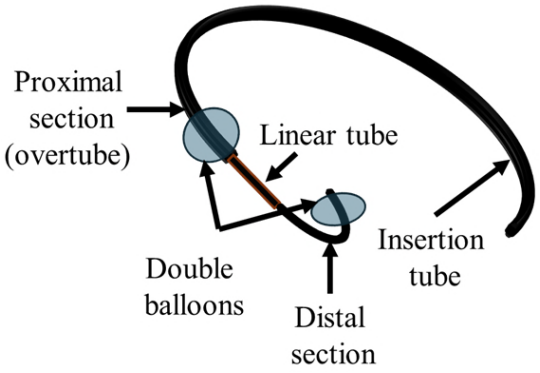


Fig. 1: Traditional design of double balloon colonoscope.

A multi-section, self-propelled soft robot for colonoscopy was developed [9]. It used two balloons, which were fixed to the proximal and distal tips of the robot. Based on the wave locomotion technique under support of balloons, the robot succeeded to move forward and backward using an acrylic tube successfully. However, it suffered from complex actuation. In [10], two cable-driven rigid sections based double balloon for colonoscopy was proposed. Each section consisted of a series-connected rigid rings and coil spring as a backbone. A linear cylinder is used to push the colonoscope out of overtube. The results demonstrated that the bending angle of the inner and outer tubes reached 90° and 180°, respectively. Additionally, its payload capacity reached 200 g. However, the prototype suffered from high friction due to rigid rings. Moreover, the actuation mechanism was sophisticated, resulted in longer insertion procedure.

The contributions of this paper are (1) proposing a novel design of a tendon-driven soft robot for colonoscopy. It is composed of two sections, each capable of bending in two planes. Additionally, the distal section is allowed to compress and extend, mimicking the behavior of a soft spring. (2) Conducting a design analysis to investigate the effect of

[1]*Department of Mechanical and Aerospace Engineering, Faculty of Science and Technology, Tokyo University of Science ibrahim.seleem@rs.tus.ac.jp

[2]Department of Industrial Electronics and Control Engineering, Faculty of Electronic Engineering, Menoufia University, Egypt (On leave) ebrahim.selim@el-eng.menofia.edu.eg

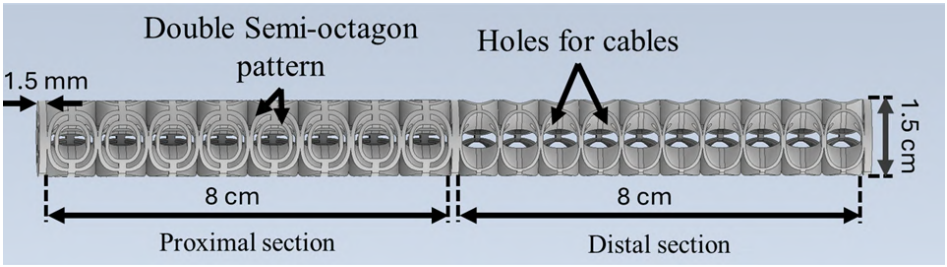


Fig. 2: Structural design of extensible prototype

modifying design parameters while considering safety and deflection. Additionally, a nonlinear static analysis is carried out to explore the bending capabilities of the proposed design under the applied force. (3) Validating the prototype experimentally, concerning its bending, compression/extension, and payload capabilities. This article represents the first phase of utilizing the compliant properties of soft material to improve the colonoscopy procedure.

The remainder of the article is arranged as follows. The design structure and working principle is discussed in section II. A detailed description Finite Element Analysis (FEA) is introduced in section III. Section IV presents the discussion and experimental validation. Finally, conclusion and future work is discussed in sectionV.

## II. Structural design

A honeycomb pattern is a geometric repeated arrangement of hexagonal cells, inspired by the natural design of beehives. Due to its excellent strength-to-weight ratio, flexibility and structural integrity, it is widely utilized in aerial vehicles and soft actuator [11], [12]. In this paper, a semi-octagon honeycomb patterns are selected to be the main structural units. Figure 2 illustrates that the design is composed of proximal and distal sections; each length is 8 cm and diameter is 1.5 cm. A 1.5 mm soft base is distributed a long the prototype to anchor cables. The proximal section consists of double patterns embedded with each other, to enhance the payload capacity of robot. On the other hand, its distal section has single pattern to allow both bending and/or extension and compression.

Bending capability of each section is controlled through four cables, spaced by 90° around the robot's body, as illustrated in Fig. 3a. Each pair of parallel cables is anchored from one end to the section's tip, while the other ends are fixed to a DC motor via a double-groove pulley. As the motor rotates, any decrease in one cable's length is equally compensated by an increase in the corresponding cable. Additionally, another four tendons are connected to the robot's distal tip, with their opposite ends fixed to a DC motor, allowing compression and extension. Moreover, they prevent the robot from twisting under compression. The prototype is 3D printed from NinjaFlex-1.75mm soft filament, as shown in Fig. 3b, due to its superior mechanical properties and durability.

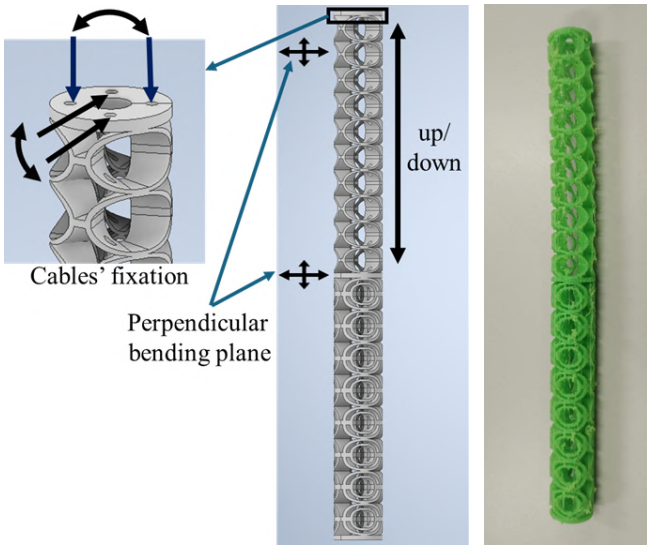


(a) (b)

Fig. 3: (a) Arrangement of wires for bending., and (b) Soft prototype.

### A. Working principle

Double Balloon Colonoscopy (DBC) is an advanced endoscopic method designed to enhance colon accessibility, particularly in cases with excessive looping or strictures [13]. The working principle of DBC depends on a controlled sequence of inflation and deflation of two balloons to hold the position of the robot, facilitating insertion and advancement of the colonoscope. Balloons are fixed to the end of each section.

The working principle of our design is illustrated in Fig. 4. Before insertion, the proximal section is fully compressed to improve the robot's stiffness, which is achieved by tensioning four wires responsible for compression, as shown in Fig. 4a. After insertion, a balloon at the end of the proximal section is inflated, acting as an anchor within the colon, as depicted in Fig. 4a. Then, figure 4b shows that the proximal section is fully extended through releasing tendons. After that, the distal balloon is inflated while simultaneously deflating the proximal section's balloon, as shown in Fig. 4c. By advancing the colonoscope and re-compressing the distal section again, the robot can move forward, as illustrated in Fig. 4d. This sequence is repeated until the robot reaches the cecum. The robot can also perform bending during insertion.

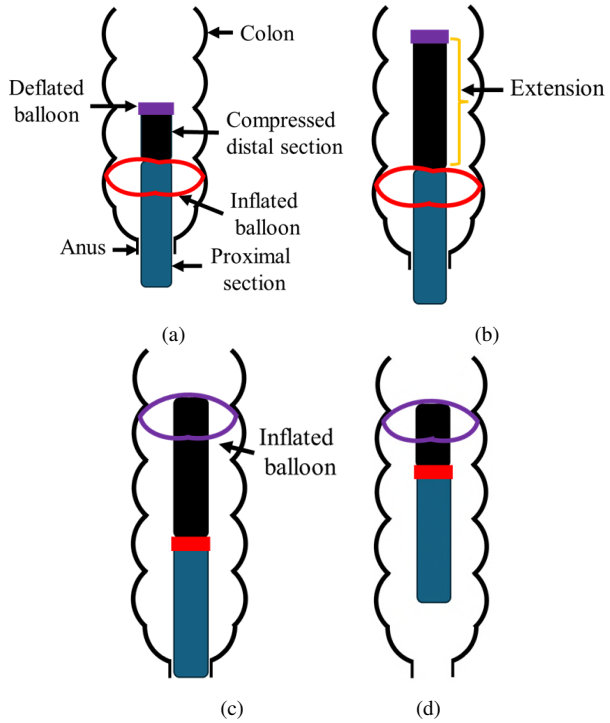


Fig. 4: Steps for soft colonoscope insertion.

A future plan will be prepared to conduct a real insertion using a colon training kit.

## III. Finite Element Analysis

Finite Element Analysis (FEA) represents a major simulation tool, which is used to assess the performance of a design under external forces and resulting deflection. Additionally, it minimizes manufacturing costs by enabling design modifications for improving its efficiency [14]. In this section, two analyses are conducted. Firstly, a design analysis is carried out to investigate the effect of modifying structural parameters while respecting the resulting stress and deflection. Secondly, a nonlinear static analysis is applied to evaluate the bending behavior under cable tension.

### A. Design analysis

The analysis starts by defining the mechanical characteristics of NinjaFlex material as depicted in Table. I. For simplicity, the analysis is applied to the distal section only.

Each pattern is formed by sketching a quarter of a semi-hexagonal shape, as shown in Fig. 5. The main pattern is obtained by mirroring this quarter horizontally and then vertically. Figure 5 illustrates that parameters $[d_1, d_2, d_3, d_4, d_5, r_1, r_2]$ are selected to carry out analysis, where $r_1$ and $r_2$ define the curvature of the pattern. The design parameters are listed in Table I.

The pressure of 0.005 MPa is applied vertically to the robot's tip, as shown in Fig. 6a. Finally, a fixed constraint is attached to the robot's base. Figures 6a, 6b, and 6c illustrate that the maximum stress values in each case are 0.9985 MPa, 0.9393 MPa, and 2.016 MPa, respectively.

| Material properties (NinjaFlex) | | Density | Young's Modulus | Tensile strength |
|---|---|---|---|---|
| | | 1040 $Kg/m^3$ | 12 MPa | 4 MPa |
| Design parameters | | | | |
| | | Case 1 | Case 2 | Case 3 |
| Variables | $d_1$ [mm] | 0.75 | 0 | 0 |
| | $d_3$ [mm] | 1.5 | 0.75 | 0.5 |
| | $d_3$ [mm] | 0.75 | 0.75 | 0.5 |
| | $d_4$ [mm] | 0.75 | 0.75 | 0.5 |
| | $d_5$ [mm] | 1.5 | 1.5 | 1 |
| | $r_1$ | 3 | 3 | 4 |
| | $r_2$ | 4 | 4 | 4 |
| Results | | | | |
| Stress [MPa] | | 0.9958 | 0.9393 | 2.016 |
| Displacement [mm] | X | 1.76 | 2.425 | 0.5038 |
| | Y | 6.799 | 7.8 | 13.94 |
| | Z | 1.321 | 1.756 | 0.501 |

TABLE I: Design variables and results

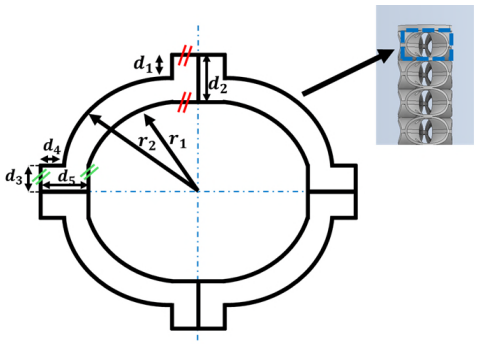


Fig. 5: Structural design of extensible prototype

The results demonstrate that the design in Case 2 is safer compared to Cases 1 and 3 under the applied pressure. On the other side, their vertical deflections are 6.799 mm, 7.8 mm, and 13.94 mm. The design in Case 3 exhibits a higher compression/extension ratio compared to Cases 1 and 2.

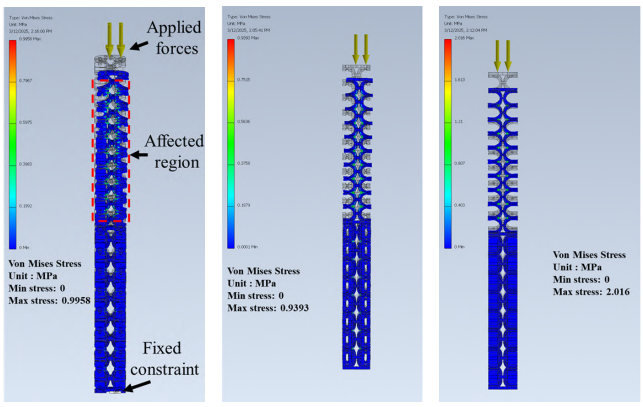


Fig. 6: Stress and displacement analysis at (a,d) Case 1., (b,e) Case 2 and (c,f) Case 3

Accordingly, the primary design in this paper is chosen to be in Case 3. It is worth noting that the deflection reflects a realistic movement of the robot.

### B. Nonlinear analysis

Due to the elastic behavior of soft material, linear static analysis is not a reliable method for accurately describing the bending of the design. Subsequently, a nonlinear static analysis is carried out to explore the performance of the design. The third-order Yeoh hyperelastic model is utilized for this study. The strain energy density for this model is computed as follows:

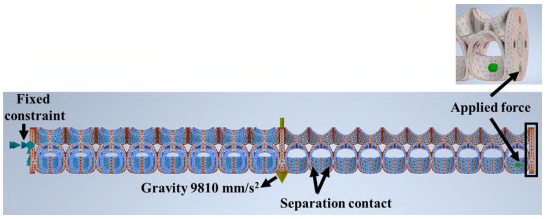


Fig. 7: The nonlinear static analysis setup.

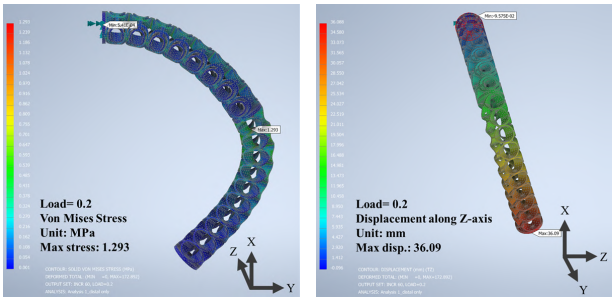


(a) (b)

Fig. 8: (a) Von Mises stress, and b) displacement along z-axis, under applied force of 0.2 N.

| | Load [N] | Displacement [mm] | | | | | |
|---|---|---|---|---|---|---|---|
| | | X | | Y | | Z | |
| | | min | max | min | max | min | max |
| Main design | 0.2 | -118.20 | 0.04 | -131.40 | 2.33 | -0.09 | 36.09 |
| Design (backbone) | 0.2 | -111.6 | 0.65 | -63.9 | 1.93 | -1.23 | 0.20 |

TABLE II: Numerical results of static analysis

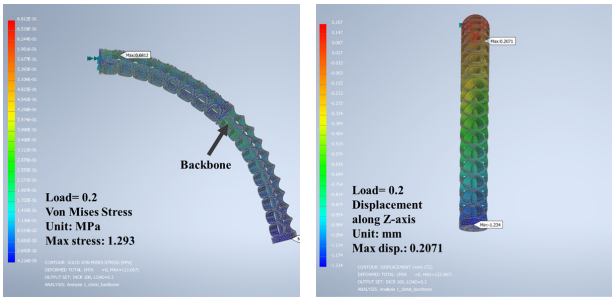


(a) (b)

Fig. 9: The resulted FEA analysis (a) Von Mises stress, and b) displacement along z-axis.

$$W = \sum_{i=1}^{3} C_{i0} \left(I_1 - 3\right)^i \tag{1}$$

where $C_i0$ are material constants and $I_1$ is the Cauchy-Green deformation tensor. As presented in [15], the constants are chosen as $C_{10} = 1.653$, $C_{20} = 0.0324$, and $C_{30} = 0.000486$.

The simulation is conducted using Inventor-NASTRAN 2024. The simulation settings are mesh element size = 1 mm, number of increments = 1000, and frictionless separation contact between each two opposite patterns, as illustrated in Fig. 7. A fixed constraint is attached to the design base, and an external force is applied to one side of its distal tip, resembling a cable tension. Figure 8a illustrates that the maximum stress is 1.293 MPa and concentrated at the base of the proximal section, under the applied force of 0.2 N. The corresponding displacements in Cartesian space are listed in the table. II. Due to the structural difference of proximal and distal sections, the maximum deflection along the Z-axis is 36.09 mm, as shown in Fig. 8b.

To tackle this challenge, a soft backbone is implemented within the structure of the prototype, as depicted in fig. 9a. It is anchored to the end of the distal section and moves freely under bending and/or compression. Similarly, the FEA analysis is repeated. The maximum stress is 0.6812 MPa under 0.2 N, as depicted in Fig. . The maximum displacement along the Z-axis is 0.20 mm, as shown in Fig. 9b. The results demonstrate the maximum stress is concentrated at the proximal section's base, enhancing the design safety and avoiding deviation under the applied force. However, it leads to lower flexibility compared to the previous configuration.

## IV. Results and Discussion

The performance of the prototype is evaluated through conducting a series of experiments concerning its bending and payload capability. Figure 10 illustrates the experimental setup, which is composed of an Arduino Mega-2560 as the main control unit, five 12-V DC motors, and their drivers. Nylon-coated stainless steel cables with a diameter of 0.3 mm are used to regulate bending and/or compression/extension of the robot. Motion of each section is controlled by four wires; each pair is connected through a

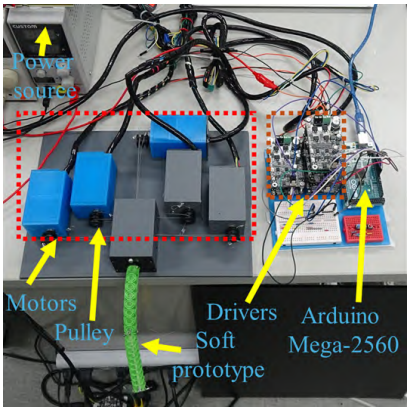


Fig. 10: Experimental setup

pulley to a DC motor, which is responsible for bending in a specific plane. Each two antagonistic tendons are connected to a double-groove pulley. During bending, the length of one cable increases while the other shortens equally. The fifth DC motor is responsible for controlling the compression and extension of the distal section, relying on four cables, each anchored at one end to its distal tip and at the other to a motor via a pulley. It is assumed that all four tendons contract and extend proportionally.

### A. *Bending phase*

Figure 11 illustrates the bending capability of the prototype while applying tension to its proximal and distal sections, respectively. The results show that it can bend up to 180° as depicted in 11a. On the other hand, the bending angle of the distal section exceeds 270°, as shown in Fig. 11c, allowing the robot to perform complex motion.

The distal section contracts by tensioning four cables simultaneously, as depicted in Fig. 12a. Under full compression, its length approximates 2.5 cm. After releasing cables, the top section retur6ans ba6ck to its original length, which is 8 cm, as shown in Fig. 12b. Moreover, the prototype successfully achieved an S-shape through the differential tensioning of cables, as illustrated in Fig. 13.

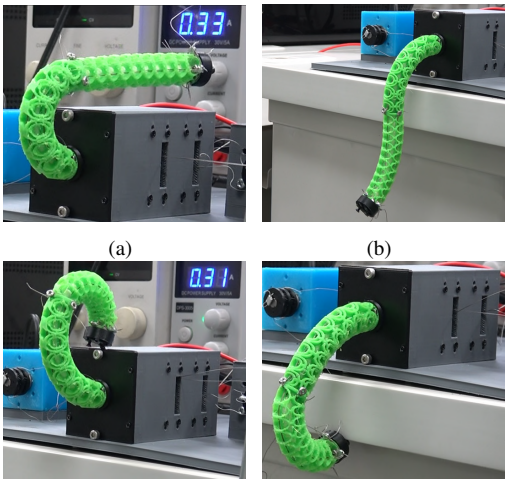

(a) (b) (c) (d)

Fig. 11: Bending capability of (a, b) the proximal section, and (b) the distal section.

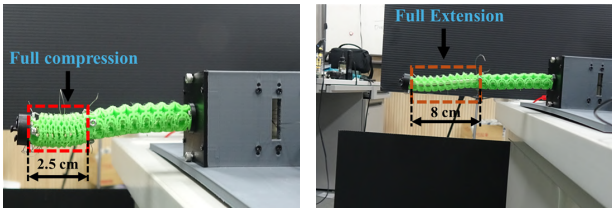


(a) (b)

Fig. 12: Compression and extension of proximal section.

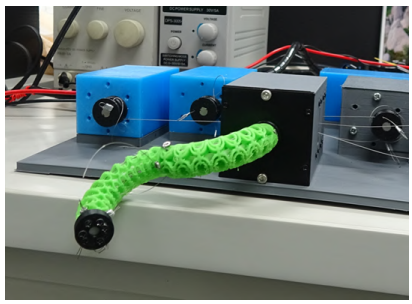

Fig. 13: Forming S-shape of two section soft robot.

### B. *Payload capacity*

Testing the prototype's payload capacity is crucial for evaluating its strength under external loads. In this experiment, weights of 20 g and 50 g are attached to the robot's distal tip, as shown in Fig. 14a and 14d, respectively. The robot was then allowed to bend, as depicted in Fig. 14b and 14e, respectively. The results indicate that the prototype successfully achieved uniform bending under 20 g and 50 g, as demonstrated in Fig. 14c and Fig. 14f, respectively. (See supplementary material.)

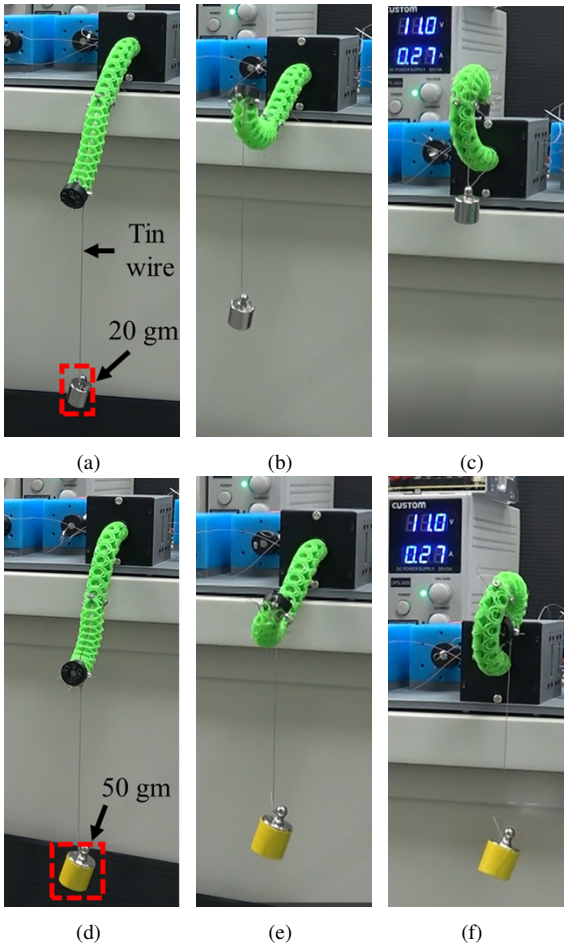


(a) (b) (c) (d) (e) (f)

Fig. 14: Payload capability of the prototype under external payload (a) 20 g and (b) 50 g.

## V. CONCLUSIONS

This paper presents the initial phase of designing a two-section soft robot for colonoscopy. The design is composed of two series-connected sections, which are built based on the semi-octagon honeycomb patterns owing to their unique flexibility and longevity. Each section is capable of bending in two planes based on tension and retraction of four cables. Each pair of parallel tendons connected to a DC motor through a pulley. On the other side, the distal section imitates a soft spring, allowing it to achieve compression and extension by using four independent cables attached to a fifth DC motor. A design analysis is carried out to investigate the effects of modifying the pattern parameters on the performance of the design. Additionally, the bending capability of the prototype is validated by conducting a nonlinear static analysis based on the Yeoh model. The simulation results show a lateral deflection under external force. To address this challenge, a soft backbone is used to improve stability and avoid unexpected movements. The robot's performance is experimentally evaluated in terms of bending and payload capacity. The results show that the robot can achieve a 270° bending angle while carrying external payloads of 20 g and 50 g, respectively. Furthermore, it achieves dexterous bending successfully. Future plans will be conducted to perform the insertion procedure using a colon training kit.

## REFERENCES


[1] K. Katanoda, T. Matsuda, A. Matsuda, A. Shibata, Y. Nishino, M. Fujita, M. Soda, A. Ioka, T. Sobue, and H. Nishimoto, "An updated report of the trends in cancer incidence and mortality in japan," *Japanese journal of clinical oncology*, vol. 43, no. 5, pp. 492–507, 2013.

[2] T. Shinagawa, T. Tanaka, H. Nozawa, S. Emoto, K. Murono, M. Kaneko, K. Sasaki, K. Otani, T. Nishikawa, K. Hata, *et al.*, "Comparison of the guidelines for colorectal cancer in japan, the usa and europe," *Annals of gastroenterological surgery*, vol. 2, no. 1, pp. 6–12, 2018.

[3] S. G. Patel, J. J. Karlitz, T. Yen, C. H. Lieu, and C. R. Boland, "The rising tide of early-onset colorectal cancer: a comprehensive review of epidemiology, clinical features, biology, risk factors, prevention, and early detection," *The lancet Gastroenterology & hepatology*, vol. 7, no. 3, pp. 262–274, 2022.

[4] J. Zhang, Y. Liu, J. Tian, D. Zhu, and S. Prasad, "Design and experimental investigation of a vibro-impact capsule robot for colonoscopy," *IEEE Robotics and Automation Letters*, vol. 8, no. 3, pp. 1842–1849, 2023.

[5] M. Shimatani, T. Mitsuyama, T. Yamashina, M. Takeo, S. Horitani, N. Saito, H. Matsumoto, M. Orino, M. Kano, T. Yuba, *et al.*, "Advanced technical tips and recent insights in ercp using balloon-assisted endoscopy," *DEN open*, vol. 4, no. 1, p. e301, 2024.

[6] H. Yamamoto, "Small bowel: Device-assisted endoscopy," *Dig Endosc*, vol. 34, no. Suppl 2, pp. 79–82, 2022.

[7] Y. Li, J. Peine, M. Mencattelli, J. Wang, J. Ha, and P. E. Dupont, "A soft robotic balloon endoscope for airway procedures," *Soft Robotics*, vol. 9, no. 5, pp. 1014–1029, 2022.

[8] T. L. Pan, M. C. Lei, W. Y. Ng, and Z. Li, "Analytical modeling of the interaction between soft balloon-like actuators and soft tubular environment for gastrointestinal inspection," *Soft Robotics*, vol. 9, no. 2, pp. 386–398, 2022.

[9] T. T. Nguyen, D. Q. Nguyen, *et al.*, "Soft robot employing a series of pneumatic actuators and distributed balloons: Modeling, evaluation, and applications," *IEEE Transactions on Robotics*, 2024.

[10] T. Takamatsu, Y. Endo, R. Fukushima, T. Yasue, K. Shinmura, H. Ikematsu, and H. Takemura, "Robotic endoscope with double-balloon and double-bend tube for colonoscopy," *Scientific reports*, vol. 13, no. 1, p. 10494, 2023.

[11] O. A. Ganilova and J. J. Low, "Application of smart honeycomb structures for automotive passive safety," *Proceedings of the Institution of Mechanical Engineers, Part D: Journal of Automobile Engineering*, vol. 232, no. 6, pp. 797–811, 2018.

[12] F. Xie, X. Hou, T. Sheng, R. Li, and Z. Deng, "Harnessing pattern transformation of honeycomb structures for soft actuators design," *Composites Part B: Engineering*, p. 112217, 2025.

[13] J. T. Koh, L. K. Wei, C. P. Francisco, R. Ravi, W. Chan, C. Khor, and R. Asokkumar, "Double balloon enteroscopy versus single balloon enteroscopy: A comparative study," *Medicine*, vol. 103, no. 20, p. e38119, 2024.

[14] K. Yang, Q. Jia, C. Feng, J. Huang, G. Chen, and Z. Yang, "Force model of robot bone grinding based on finite element analysis," *Measurement*, vol. 243, p. 116124, 2025.

[15] H. K. Yap, H. Y. Ng, and C.-H. Yeow, "High-force soft printable pneumatics for soft robotic applications," *Soft Robotics*, vol. 3, no. 3, pp. 144–158, 2016.